Direct observation of dynamic crossover in fragile molecular glass formers with 2D IR vibrational echo spectroscopy

David J. Hoffman, Kathleen P. Sokolowsky, and Michael D. Fayer[a)]
Department of Chemistry, Stanford University, Stanford, California 94305, USA

(Received 12 January 2017; accepted 22 February 2017; published online 31 March 2017)

The dynamics of supercooled liquids of the molecular glass formers benzophenone and *ortho*-terphenyl were investigated with 2D IR spectroscopy using long-lived vibrational probes. The long lifetimes of the probes enabled structural dynamics of the liquids to be studied from a few hundred femtoseconds to a nanosecond. 2D IR experiments measured spectral diffusion of a vibrational probe, which reports on structural fluctuations of the liquid. Analysis of the 2D IR data provides the frequency-frequency correlation function (FFCF). Two vibrational probes were examined with equivalent results, demonstrating the observed liquid dynamics are not significantly influenced by the probe molecules. At higher temperatures, the FFCF is a biexponential decay. However, at mild supercooling, the biexponential decay is no longer sufficient, indicating a dynamic crossover. The crossover occurs at a temperature well above the mode-coupling theory critical temperature for the given liquid, indicating dynamic heterogeneity above the critical temperature. Examination of the low temperature data with lifetime density analysis shows that the change is best described as an additional, distinct relaxation that shows behavior consistent with a slow β-process. *Published by AIP Publishing.* [http://dx.doi.org/10.1063/1.4978852]

I. INTRODUCTION

Supercooled liquids have a host of intriguing but not well-understood static and dynamic properties that have made them an important subject of both experiment and theory.[1–11] Above their melting points, these liquids display standard liquid-like behavior: independent, exponential relaxations and transport properties that follow Arrhenius temperature dependences. As the temperature is decreased towards the glass transition, these properties smoothly become more glass-like, with sharply slowing transport properties, dynamical heterogeneity, and complex, collective relaxation behavior. Explaining the physical, microscopic origin of this intermediate transition has been a principal goal of theories of the glass transition.

Mode coupling theory (MCT),[6,7] the most successful first-principles treatment of the glass transition, has been used for decades to model high-temperature glassy dynamics. As the homogeneous, hydrodynamic MCT equations break down at the critical temperature T_c ($\sim 1.2T_g$, where T_g is the glass transition temperature), this temperature has been associated with the crossover between liquid-like and glass-like behavior, and thus the emergence of the more exotic behavior of supercooled liquids. T_c has been assigned to changes in the potential energy landscape and the onset of activated dynamics,[1–3,7,12] the separation of the Johari-Goldstein slow β-relaxation from the even slower α-relaxation,[3,4,13–16] and the decoupling of transport coefficients and dynamic heterogeneity.[15,17–20]

Relatively recent computational work has shown that the "onset temperature" T_o, a temperature above T_c defined as the start of super-Arrhenius temperature dependence in the α-relaxation, is at least as important as T_c in describing glassy phenomena.[21–24] In terms of the potential energy landscape description of the glass transition,[21,22,25] above T_o, the liquid is unaffected by the underlying landscape and behaves like a normal liquid. Below T_o but above T_c, the liquid first becomes "landscape influenced." Some particles do not have enough energy to escape potential energy minima independently, and glassy dynamics such as activated processes, heterogeneity, and transport property decoupling first appear. T_c is then a final crossover, as the liquid becomes "landscape dominated" and the glassy relaxation pathways become the only ones available.

Here we present 2D IR vibrational echo spectroscopy data on the fragile glass forming liquids (see Figure 1) benzophenone (BZP) and *ortho*-terphenyl (OTP), two of the most studied fragile molecular glass formers. BZP and OTP have both been studied by Optical Kerr effect (OKE),[26–29] light scattering,[30–36] calorimetry,[37,38] and dielectric spectroscopy,[14,39–43] while OTP has also been studied by Nuclear Magnetic Resonance (NMR),[19,44] neutron scattering,[45–47] and some less common techniques.[20,48–51] The wealth of information on these two liquids provides valuable background and context for interpreting the 2D IR spectroscopy results, which provide new information and insights.

2D IR spectroscopy measures spectral diffusion experienced by non-perturbative vibrational probes in the glass forming liquids, which in turn provides direct information on the structural dynamics of the liquids on fast time scales.[52–54] The variety of local liquid structures results in a range of transition frequencies of the vibrational mode of the probe. The range of frequencies gives rise to the inhomogeneously broadened spectral line shape observed by infrared absorption spectroscopy. As the liquid structures evolve with

[a)]Email: fayer@stanford.edu. Telephone: 650 723-4446.

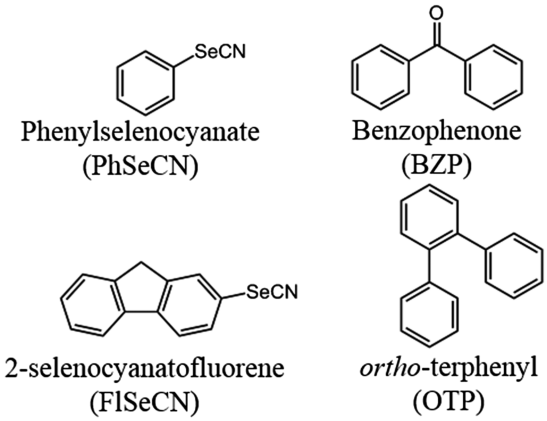

FIG. 1. Molecular structures of the supercooled liquids and the vibrational probes.

time, the resonant frequency of a probe vibration changes, sampling frequencies within the inhomogeneously broadened line. The time evolution of the vibrational frequencies is called spectral diffusion, which is measured with 2D IR spectroscopy by observing the time evolution of the 2D line shape. As 2D IR tracks the time evolution of spectral properties, it maintains partial time ordering in its response functions.[52] This feature is lost in pure frequency domain spectroscopy, as all permutations of time ordering contribute in their frequency-domain analogue. The mixed frequency and time domain representation permits clear interpretations of the complex dynamics found in condensed phases.

Supercooled liquid dynamics cover an extremely broad range of time scales, making them difficult to study. While 2D IR spectroscopy is well-suited for studying picosecond-scale dynamics, most vibrational modes have lifetimes of at most a few tens of picoseconds, severely limiting the measurement of slower dynamics. The development of long-lived selenocyanate probes has been an important advance, as their nitrile stretches can have lifetimes of many hundreds of picoseconds, permitting the collection of data from <1 ps to ~1 ns. These probes have previously been used in 2D IR spectroscopy to probe dynamics in liquid crystals,[55,56] in solvation shells of water and ionic liquids,[57–59] and in proteins.[60] It has been shown that the spectral diffusion reported by probes of similar shape and size as the molecules that make up the bulk liquid is nearly identical to that felt by natural vibrational probes that are intrinsic to the liquid itself.[55,61]

Below, we demonstrate that 2D IR vibrational echo spectroscopy can detect a dynamic crossover at a temperature T_o that is distinct from the MCT critical temperature T_c. At high temperatures, the observed spectral diffusion relaxes as a biexponential decay. The fast component is unambiguously indicative of ultrafast, picosecond-scale dynamics that are largely independent of temperature. The slow component can be shown to demonstrate the same super-Arrhenius temperature dependence as the α-relaxation[2,3]—the complete orientational relaxation of the liquid—as observed with other spectroscopic techniques. The crossover appears as a systematic deviation in the fit from the biexponential decay function used to model the relaxation of the high-temperature liquid, indicating a change in the relaxation process to a more complex functional form. The temperature where this crossover occurs is well above the temperature T_c that can be determined from the temperature dependence of the relaxation rates of the data with MCT and is consistent with the theoretical and computational descriptions of the onset temperature T_o.[21,22]

A description of the nature of the crossover is more ambiguous. Analysis of the data using Lifetime Density Analysis (LDA),[62] functionally a numerical inverse Laplace transform, suggests that this crossover may manifest as the appearance of an additional, β-like relaxation process, which is commonly associated with the existence of activated dynamics, as opposed to a simple broadening in the distribution of relaxation rates. This possibility is considered in the context of the connection of the slow β-relaxation process to fast density fluctuations, which 2D IR spectroscopy is well suited to study, the onset of dynamic heterogeneity, and rotational-translational decoupling that theory and simulation have shown to occur at T_o. The observed Arrhenius thermodynamics of the new relaxation process is also consistent with the existence of non-"landscape influenced" particles between the temperatures T_o and T_c, as described in the potential energy landscape model of the glass transition.

II. EXPERIMENTAL PROCEDURES

A. Sample preparation

BZP and OTP were purchased from TCI America and phenyl selenocyanate (PhSeCN, see Figure 1) was purchased from Sigma Aldrich. 2-selenocyanatofluorene (FlSeCN, see Figure 1) was synthesized in one step from 2-aminofluorene according to analogous literature procedures.[55,63] Full details of the synthesis and characterization can be found in the supplementary material. BZP and OTP were further purified by vacuum distillation before use. Solutions of 5 mol. % PhSeCN in BZP, 5 mol. % PhSeCN in OTP, and 2 mol. % FlSeCN in BZP were prepared.

For the IR experiments, the solutions were heated to ~50 °C and loaded between two 3 mm CaF_2 windows separated by a 190 μm Teflon spacer. The windows were contained in a copper cell to allow for optimal thermal conduction. The cell temperature was varied from 248 K to 385 K with a Peltier thermoelectric device. Proportional-integral-differential (PID) control kept temperatures to within ±0.05 K. For ultrafast infrared experiments at temperatures below the T_c of the respective samples, both BZP and OTP solutions showed an enhanced tendency to crystallize. Avoiding this issue required frequent cycling of temperatures to melt and recool the samples mid-experiment, limiting effective temperature control to ±0.5 K.

B. Differential scanning calorimetry (DSC)

Differential scanning calorimetry (DSC) experiments were performed with a Q2000 DSC (TA Instruments) to quantify how the presence of the probe molecules affected the thermodynamic observables T_m and T_g. Approximately 5 mg of the sample solutions was loaded as a solid into Tzero standard pans. The samples were run through simple heat-cool-heat

routines at ramp rates of 10 K/min to determine thermodynamic properties. T_m was measured as the temperature at the peak of the melting event. T_g was measured as the midpoint temperature of the sudden increase in heat capacity on heating.

C. FT-IR spectroscopy

FT-IR experiments were performed on a Nicolet 6700 FT-IR spectrometer (Thermo-Fisher Scientific) at 1 cm^{-1} resolution. Although both BZP and OTP have minimal IR absorption in the range of interest (between 2130 and 2170 cm^{-1}, the region where the 0-1 and 1-2 transitions for the nitrile stretch in the selenocyanate probes occurs), background subtraction of the neat BZP and OTP spectra was performed for the doped systems to isolate the nitrile stretches of the selenocyanate probes for analysis. Voigt functions were used to fit the line shapes.

D. Ultrafast infrared spectroscopy

The methods and laser setup employed in the ultrafast infrared experiments have been described in detail previously.[54,64] To summarize, a Ti:Sapphire oscillator and regenerative amplifier produced ultrafast pulses at 800 nm. These pulses pumped an optical parametric oscillator (OPA) that converted the light to the mid-IR (4.6 μm). The mid-IR pulses had energy of ~6 μJ/pulse at a 1 kHz repetition rate, a bandwidth of 90 cm^{-1}, and a duration of ~125 fs. The pulses are controlled temporally to an accuracy <0.1 fs through the use of mechanical delay stages, which provided a potential experimental window of ~2 ns.

For pump-probe experiments, used in this paper for determination of vibrational lifetimes, each pulse is split into a strong pump pulse and a weak probe pulse. The polarization of the probe is rotated relative to the pump to derive population and orientational information from the samples. The pump and probe pulses were crossed in the sample, and the probe transmission signal was dispersed and collected on a 32 element mercury-cadmium-telluride array detector with respect to time. The probe was polarized either parallel or perpendicular relative to the pump. The intensities of these decays are given by

$$\begin{aligned} I_{||} &= P(t)(1 + 0.8C_2(t)) \\ I_{\perp} &= P(t)(1 - 0.4C_2(t)), \end{aligned} \tag{1}$$

where $P(t)$ is the vibrational population relaxation and $C_2(t)$ is the second Legendre polynomial correlation function (orientational correlation function for a dipole optical transition). From these two measurements $P(t)$ can be determined,

$$P(t) = \frac{I_{||} + 2I_{\perp}}{3}, \tag{2}$$

and while not discussed in this work, $C_2(t)$ can be similarly extracted,

$$r(t) = 0.4C_2(t) = \frac{I_{||} - I_{\perp}}{I_{||} + 2I_{\perp}}. \tag{3}$$

Perpendicularly polarized echo experiments described below show that temperature dependent characterization of $C_2(t)$ is not necessary for characterization of structural spectral diffusion (SSD).[65,66]

For vibrational echo experiments, each pulse is split into four pulses. The first three pulses, of roughly equal intensity, are overlapped spatially in the sample in BoxCARS geometry to generate the vibrational echo signal pulse that propagates in a unique direction. The fourth, much weaker pulse, serves as a local oscillator (LO), which is overlapped spatially and temporally with the echo before reaching the array detector. Mixing the echo with the LO provided heterodyne detection that gives necessary phase information and amplifies the echo signal. The delay time (τ) between pulses 1 and 2 is scanned while holding the delay time (T_w) between pulses 2 and 3 constant, generating a time-domain interferogram on each pixel of the array detector. The use of the quasi-rotating frame method[67] permitted faster collection of individual interferograms by permitting larger τ step sizes, going from approximately 4 fs to 75 fs time steps. A numerical Fourier transform of the interferograms yields the 2D IR spectra for that T_w, where the horizontal axis frequencies (ω_τ) are derived from the FT while the vertical axis frequencies (ω_m) are given by the 32 pixels of the array monochromator (see Figure 2).

The echo experiment in effect "labels" the initial frequencies of the probes with pulses 1 and 2. During the delay time T_w, the liquid structure evolves causing spectral diffusion to occur. Pulse 3 generates the echo signal which reports on the final frequencies of the probes. The 2D IR spectrum shows the

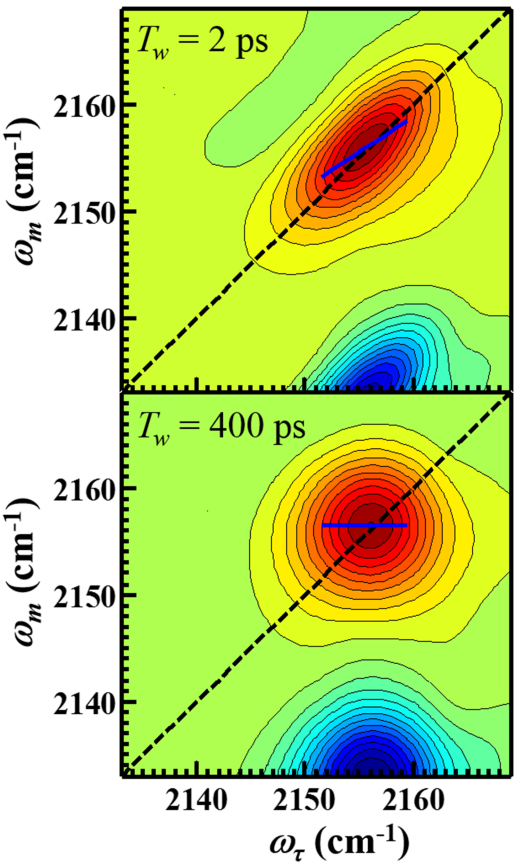

FIG. 2. Sample 2D IR spectra of PhSeCN in BZP at 288 K at waiting times (T_w) of 2 ps (top) and 400 ps (bottom). The change in shape of the 2D spectrum with T_w is related to the liquid dynamics. The dashed black line is the diagonal. The blue lines are the center lines. The slopes of the center lines as a function of T_w give the normalized FFCF.

correlation between the initial (ω_τ) and the final (ω_m) frequencies. When the waiting period T_w is short (top panel Figure 2) relative to structural rearrangements in the liquid, the initial and final frequencies are highly correlated, resulting in a 2D spectrum that is elongated along the diagonal (dashed lines in Figure 2). At long T_w (bottom panel Figure 2), the liquid structure has evolved substantially causing the initial and final frequencies to lose correlation, resulting in a rounder spectrum (bottom panel Figure 2). The correlation of the initial and final frequencies can be quantified with the center line slope (CLS) method.[54,68] The blue lines in Figure 2 are the center lines. As T_w is increased, the slope of the center line changes from a maximum value of 1 to 0 when all correlation has been lost because all liquid structures have been sampled. 2D spectra are taken over a range of T_w's. A plot of the slopes of the center lines vs. T_w, CLS(T_w), is the normalized frequency-frequency correlation function (FFCF).

Spectral diffusion is quantified by the FFCF. The FFCF is the probability that an oscillator with a given initial frequency will have that same frequency at a later time, averaged over all of the initial frequencies in the inhomogeneous line shape. A simplified Kubo model can be applied to the FFCF,[69]

$$C(t) = \langle \delta\omega(t)\delta\omega(0)\rangle = \sum_i \Delta_i^2 \exp(-t/\tau_i), \tag{4}$$

where Δ_i and τ_i are the frequency fluctuation amplitude and time constant of the ith dynamical component. The normalized FFCF can be readily extracted from the 2D spectra through the use of the CLS method.[68,70] The full FFCF with the Δs in frequency units, including the time dependent inhomogeneous and time independent homogeneous contributions, is obtained by combining the CLS(T_w) with the linear absorption spectrum taken with FT-IR.[68,70]

The desired information is the time dependence of the structural evolution of the liquid. The possibility of significant impact on the measured dynamics from probe rotation, i.e., from rotationally induced spectral diffusion (RISD),[65,66] was eliminated via polarization studies. Briefly, the sample was studied using both the standard, "parallel" configuration $\langle XXXX\rangle$ and a "perpendicular" configuration $\langle XXYY\rangle$, where the first two pulses are polarized 90° relative to the latter two. In the presence of RISD, the $\langle XXYY\rangle$ configuration will have systematically faster relaxation than $\langle XXXX\rangle$. If RISD occurs, it can be separated from the desired structural spectral diffusion (SSD) using measurements of the rotational anisotropy of the probe and established theoretical procedures. For both PhSeCN and FlSeCN, the FFCFs obtained from the two polarization schemes were identical within experimental error (see the supplementary material), thus eliminating the rotational dynamics of the probe as a significant source of the measured spectral diffusion.

III. RESULTS AND DISCUSSION

A. Differential scanning calorimetry

Differential Scanning Calorimetry (DSC) measurements were taken to quantify how the presence of the probe molecules affected the thermodynamic observables T_m and T_g. In both liquids, the samples doped with PhSeCN had their melting and glass transition temperatures depressed by a few degrees relative to the pure liquids. Notably, the glass transition depression was negligible for FlSeCN in BZP, a probe designed specifically to match the structure of BZP, compared to PhSeCN in the same liquid at similar concentrations. The results are summarized in Table I.

B. FT-IR spectroscopy

Temperature dependent FT-IR spectra were taken of all three systems to observe how the nitrile stretch absorption line shape of the probe molecules changed over the range of temperatures studied (Figure 3). In all three systems, the nitrile stretch peak frequency was ~2155 cm^{-1} with a FWHM of about 10 cm^{-1}, consistent with other molecular selenocyanate probes in analogous systems.[55,56] System-specific details are summarized in Table I. Fitting the peaks to a Voigt function shows an increasing inhomogeneous linewidth and proportionately shrinking homogeneous linewidth with decreasing temperature, in accord with the detailed observations using 2D IR spectroscopy (See Tables SI–SIII in the supplementary material). The nitrile stretch frequency and line shape of all three systems were found to be largely independent of temperature, highlighting the inability of linear spectroscopy to extract dynamical information.

C. Ultrafast infrared spectroscopy

1. Fitting procedures and choice of model

In contrast to the linear FT-IR spectra, the FFCFs obtained via 2D IR vibrational echo spectroscopy of both BZP and OTP showed dramatic changes with decreasing temperature. Figure 4 shows the temperature dependence of some of the CLS(T_w) data, where T_w is the "waiting time" (time between pulses 2 and 3 in the 2D IR pulse sequence) during which the liquid structure evolves. The FFCF extracted from 2D IR data was fit with the Kubo model given in Equation (4). Each of the decay time constants obtained from the fits reflects the time scale of a distinct relaxation process. This model has had great success in fitting 2D IR data for a variety of systems including organic liquids, water, proteins, liquid crystals, and room-temperature ionic liquids.[55–59,71–75] The multiexponential model was chosen as our starting point, as above T_m, these glass forming liquids are simple organic liquids. At these higher temperatures, the CLS(T_w) decay curves for all three samples fit well to biexponential decays.

However, at temperatures where mild supercooling occurs, it was found that there were systematic errors in the fits, which were apparent in the residuals. These errors showed that a biexponential function was insufficient to characterize

TABLE I. Spectral and thermodynamic properties of studied systems.

	Probe	$\tilde{\nu}$ (cm^{-1})	FWHM (cm^{-1})	T_m (K)	T_g (K)
BZP	None	···	···	322	214 ± 1
	5 mol. % PhSeCN	2153.8	10	321	212 ± 1
	2 mol. % FlSeCN	2152.5	10	320	214 ± 1
OTP	None	···	···	331	250 ± 2
	5 mol. % PhSeCN	2155.5	9	328	245 ± 2

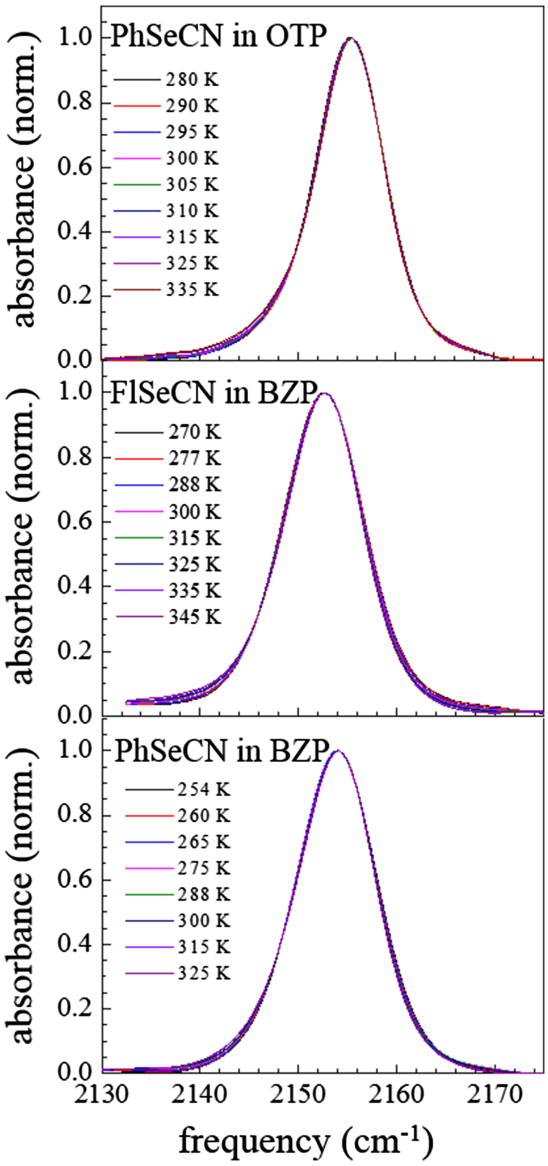

FIG. 3. Background subtracted temperature-dependent FT-IR spectra (from top to bottom) of 5 mol. % PhSeCN in OTP, 2 mol. % FlSeCN in BZP, and 5 mol. % PhSeCN in BZP showing the minimal changes in the line shapes with temperature.

the data. Two approaches were tried to address this discrepancy: following the Kubo model by fitting the data using a triexponential decay, and following other studies of glassy dynamics by replacing the second exponential with a stretched exponential,[2–4]

$$C(t) = A_1 \exp(-t/\tau_1) + A_2 \exp(-(t/\tau_2)^{\beta}), \tag{5}$$

where β is the stretching exponent, such that $0 < \beta \leq 1$, which describes a distribution of relaxation times. At $\beta = 1$, the distribution of relaxation times is infinitely narrow and the function is a biexponential decay, while as β approaches zero the distribution becomes wider. While the stretched exponential is *ad hoc* in implementation, it is a simple model that represents a distribution of relaxation times in supercooled liquids. Both of these models yield curves that adequately fit the data, so it is necessary to compare the models on statistical and physical grounds to determine which is appropriate. Full tables of fit

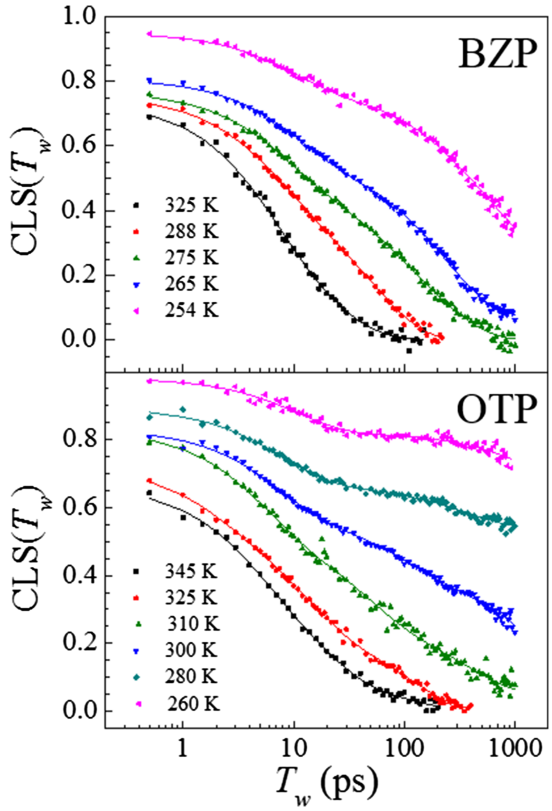

FIG. 4. Example 2D IR CLS(T_w) data (the normalized FFCF) for 5 mol. % PhSeCN in BZP and 5 mol. % PhSeCN in OTP over a range of temperatures. The data were fit with multi-exponential decays (solid lines).

parameters for both models can be found in the supplementary material.

It is important to note that the exponential plus stretched exponential and the triexponential decay models provide very similar descriptions of the relaxation of the system. As neither model affects the first exponential decay, the behavior of its amplitude and time constant (t_{fast}) shows only minor variation between the fits. The mean relaxation time of the stretched exponential is

$$\langle \tau \rangle = \frac{\tau}{\beta} \Gamma\left(\frac{1}{\beta}\right), \tag{6}$$

where Γ is the gamma function. It can be shown to be analogous to the slowest time constant (t_{slow}) from the triexponential fit. Similarly, the amplitude of the stretched component is approximately the sum of the middle and slow components' amplitudes in the triexponential model. Thus, conclusions derived from these quantities from one model can be taken over to the other model without additional analysis.

Fitting the temperature dependent data with either model shows that there is a change in dynamics that occurs at mild supercooling. In the triexponential model, this change is manifested as the appearance of the extra, intermediate decay process. In the exponential plus stretched exponential model, β is identically 1 at high temperatures, and then starts to decrease roughly monotonically with further cooling after reaching a certain temperature. The dynamical importance of the crossover temperature depends solely on the fact that it deviates from biexponential decay and is thus independent of this model choice. However, at this point, it is ambiguous as

to whether the dynamical change comes from the addition of a new relaxation process or the "smearing" of a single process over a range of relaxation times.

As the two models make significantly different predictions regarding the distribution of relaxation times, they can be tested through the use of lifetime density analysis (LDA).[62] As opposed to the discrete sum of exponentials in Equation (4), the CLS decay can be described as a Laplace transform,

$$C(t) = \int_0^\infty \Phi(\tau) \exp(-t/\tau) d\tau, \tag{7}$$

where $\Phi(\tau)$ is the spectral distribution function. In principle, a reverse Laplace transform can be performed to calculate the underlying spectral distribution. Computationally, Equation (7) is discretized to be similar to Equation (4), but with a very large number of decays. In this case, 200 lifetimes were used. The large number of exponentials allows the transform to function model independently, and can capture the nature of non-exponential decays such as the stretched exponential.

Experimental noise hinders direct application of this model to real data, so the data must be regularized to prevent overfitting. The calculations were performed with the OPTIMUS-LDA software package, which uses the commonly employed Tikhonov regularization method. To pick a regularization parameter that balances between goodness of fit and level of smoothing, a large number of parameters are tried from a wide range. At the end of the calculations, the residual norm is plotted against the smoothing norm. This plot, called the L-curve criterion, strikes a compromise between overfitting and oversmoothing at the elbow of the curve.

The spectral distribution function was calculated for those data sets where the data could not be modeled as a biexponential unambiguously, and the decay went approximately to zero within the experimental window. A sample result is shown in Figure 5 (black curve). To compare the distribution calculated for the experimental data against the two models, the calculated fit curves for both the exponential plus stretched exponential (red curve) and triexponential (blue curve) decays were run through the same process to generate their spectral distribution functions as well. As can be seen in Figure 5, three distinct peaks in the spectral distribution occur in the locations predicted by the triexponential fit. Furthermore, the width of the slowest distribution is much narrower than what is predicted by the exponential plus stretched exponential model, as the stretched peak is both shorter and broader on both sides of its peak than what is seen in the experimental data, even when the experimental data are broadened by noise. While broadening from noise is extremely common, it is unusual for additional spectral peaks to appear from the process with proper regularization. The three clear peaks, as well as the relative height and width of the slowest distribution, provide strong support for the triexponential model.

As LDA is only reliable if the entire decay is captured in the experimental window, other techniques had to be pursued to examine colder temperature data. The Akaike information criterion (AIC) was used to compare the efficacy of fit of the triexponential and exponential plus stretched exponential models to the data. A version was used that permitted comparison of

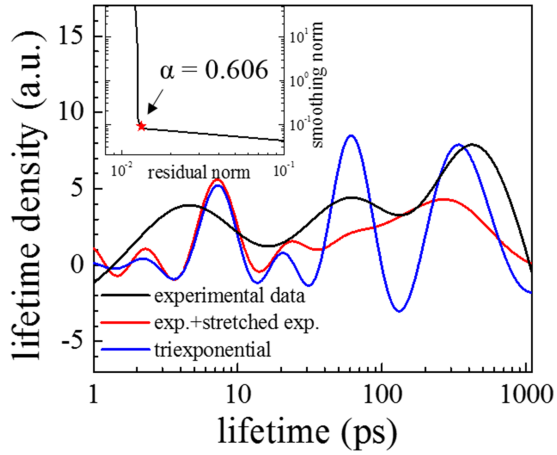

FIG. 5. Lifetime density analysis (LDA) of the CLS of 5 mol. % PhSeCN in BZP at 270 K compared to the LDA of the fit curves for the triexponential and exponential plus stretched exponential fitting functions described in Section III C 1. LDA is related to a numerical inverse Laplace transform. The three peaks predicted by the triexponential fit are clearly visible at the expected locations. While it is common for experimental noise to broaden spectral features, LDA generally does not produce additional peaks with proper regularization. Inset: L-curve criterion, showing that the regularization scheme employed strikes a balance between oversmoothing and overfitting for the experimental data. α is the regularization parameter used for Tikhonov regularization.

the models over multiple data sets.[76] Performing this procedure over 13 data sets which could not be fit to a biexponential showed that the exponential plus stretched exponential was only 0.004 times as probable as the triexponential to minimize information loss, or rather, that statistically it is 250 times more likely (2.9 σ) that the triexponential model is correct. While AIC analysis greatly favors the triexponential function over the exponential plus stretched exponential, it does not absolutely eliminate the exponential plus stretched exponential model. It does show that the triexponential model is still greatly favored despite having an additional free parameter.

The triexponential decay implicitly assigns each decay to a separate relaxation process, thus making the final decay a single exponential. Frequently in the literature, the final α-relaxation is modeled as a stretched exponential. However, the stretched exponential is an empirically derived function that describes a somewhat arbitrary distribution of relaxation rates, making its usage more customary than physically grounded. For instance, in MCT, the successful microscopic description of the approach to the glass transition, it can be readily shown that the long-time behavior of any non-glassy correlator is a single exponential.[6,7,77] Similarly, the final decay in time-domain Optical Kerr Effect (OKE) experiments is well described by a single exponential, and the entire OKE time dependent data are reproduced by schematic MCT.[28,55,56,78,79]

In arguing that the third exponential fully represents the final decay, it is necessary to establish that the first two exponentials reflect separate relaxation processes. Intermediate-time relaxation processes appear in other time-domain spectroscopy, including OKE, as a series of power laws, which have been successfully modeled theoretically using schematic MCT correlators.[56] However, these power laws are not unique to simple glass forming liquids, and appear also in other complex liquids, such as liquid crystals and ionic liquids,[56,57,80,81]

and are conspicuously absent from 2D IR experiments on these systems.[55–58] This highlights a fundamental difference in the spectral diffusion observable from other observables, in that relaxations that have complex functional forms in other techniques appear as simple exponential relaxations in 2D IR. While a full microscopic theory of spectral diffusion is lacking, it has been shown that schematic MCT correlators can describe the multi-exponential decay in liquid crystals[56] in the same way that they can describe the power law to exponential decay in OKE spectroscopy. This demonstrates that a multi-exponential decay is not forbidden by MCT theory; the same microscopic processes that generate power laws in some time-domain techniques can be manifested differently in other techniques, e.g., 2D IR, depending on the nature of the correlation functions.

On the basis of lifetime density analysis, the AIC statistical comparison of the two models, the *ad hoc* nature of the stretched exponential, the final exponential decay seen in MCT and OKE, and the ability of the schematic MCT equations to produce multiexponential decays, the triexponential model is highly favored for describing the 2D IR data in the more deeply supercooled regime. The above material demonstrates that the triexponential model is the most appropriate for describing the 2D IR data. Nonetheless, similarities and differences between the triexponential and exponential plus stretched exponential pictures will be made where appropriate.

2. Analysis with the Kubo model

Following the Kubo model (Equation (4)), the FFCFs were fit as a sum of exponential decays, where each decay corresponds to a relaxation process. The results of the fits quantify the time scales of the various relaxation processes, which are summarized in Figure 6. Full tables of the FFCF parameters are in the supplementary material. The FFCFs obtained from above the melting point through mild supercooling were fit very well with biexponential decays. At deeper supercooling, but above T_c, the FFCFs could no longer be fit with a biexponential; as discussed above, a triexponential fitting function was used to obtain fits without systematic deviations between the data and the fits. The transition from a biexponential decay to a triexponential decay indicates the emergence of a new relaxation process.

At the coldest temperatures, the slowest exponential time constant becomes too slow to extract reliably from the data, as its time scale far exceeds the experimental window of ~1 ns, which is limited by the vibrational lifetime. For the Kubo model, the data were either fit as a triexponential with the slowest time constant fixed to the extrapolated value or fit as a biexponential with a constant offset, indicating an effectively "infinite" relaxation time on the experimental time scale.

To determine if the glassy dynamics observed with the 2D IR experiments are influenced by the choice of the vibrational probe, the larger probe 2-selenocyanatofluorene (FlSeCN, see Figure 1) was synthesized. A fluorene base was selected because it is similar in structure to BZP, has limited internal degrees of freedom, and differs in size and shape from PhSeCN. FlSeCN was added at 2 mol. % to maintain a similar

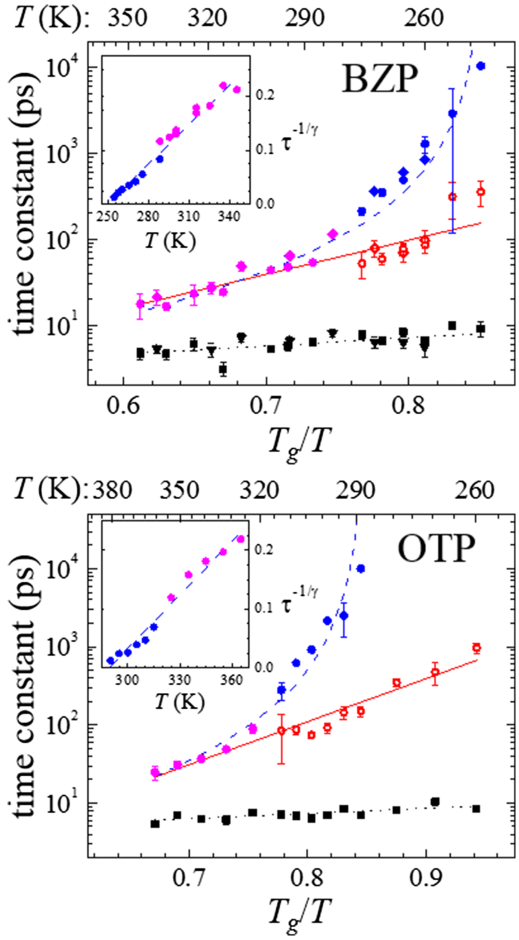

FIG. 6. Arrhenius plots of the temperature dependence of CLS(T_w) time constants of BZP (top) and OTP (bottom) obtained using the Kubo model. Circles and squares were determined using PhSeCN, diamonds and triangles using FlSeCN. t_{slow}: filled circles and diamonds (magenta: derived from biexponential; blue: from triexponential) fit to the ideal MCT scaling law (blue dashed curves). t_{mid}: open red circles and diamonds fit to Arrhenius law (red solid lines). t_{fast}: black squares and triangles fit to Arrhenius law (black dotted lines). Insets: Ideal MCT rectification diagrams, which linearize t_{slow} according to the scaling law for determination of T_c.

nitrile absorbance at room temperature as the samples with PhSeCN.

The PhSeCN vibrational probe depresses the glass transition temperature by about 2 K, while FlSeCN leaves the glass transition temperature unchanged within experimental error (see Table I). The scaling of the temperature as T_g/T removes the difference in T_g. Results from the two probes are shown in the top panel of Figure 6. The data points, circles, and squares were obtained using the PhSeCN probe and the diamonds and triangles were obtained using the FlSeCN probe. The data points from the two probes for all three time constants fall on top of each other within experimental error. While the two probes are chemically similar, the FlSeCN probe is much larger than the PhSeCN probe; these results demonstrate that the measured dynamics are independent of the vibrational probe's mass and volume, within experimental error, and instead reflect the dynamics of the liquid. When the data for the two probes are compared at the same absolute temperatures, the time constants differ by ~30%, which demonstrates the role that the distance from T_g plays in the dynamics rather than the absolute temperature.

The slowest time constant (t_{slow}), the slower biexponential time constant at higher temperatures and the slowest triexponential time constant at lower temperatures, ranges from ~15 ps to several nanoseconds. The slowest time constant has a super-Arrhenius temperature dependence, a feature most commonly seen in α-relaxation.[1–3] In addition, t_{slow} is the dominant component of the spectral diffusion in the supercooled regime, accounting for as much as 70% of the CLS decay at the lowest measured temperatures. While the measured time constant t_{slow} is nearly an order of magnitude faster than the α-relaxation times measured by other spectroscopies, the common functional form suggests a similar molecular origin. This conclusion has previously been proposed in other studies of spectral diffusion in glass formers.[71,82]

To further support the assignment of the slowest time constant to α-relaxation, t_{slow} was successfully linearized using the critical law predicted by ideal MCT (Figure 6 insets, dashed blue lines),[7,28]

$$\tau^{-1/\gamma} \propto |T - T_c|\,, \tag{8}$$

where literature values of γ (BZP: 1.92, OTP: 2.11),[28] as determined by OKE spectroscopy, were used. As the 2D IR data do not contain the power laws predicted by ideal MCT (which necessitates the use of γ from another experiment), the use of the scaling law here is a heuristic relation providing a comparison to the temperature dependence as measured by other spectroscopies rather than as part of a full theoretical description. In OKE spectroscopy, the value of γ is derived by measurement of the exponent of the temperature-independent von Schweidler power law. In analogous experiments with nematic liquid crystals, the exponent of the von Schweidler power law did not change with low concentrations of probe molecules, justifying the application of the γ exponent obtained from pure liquids to these systems that also contain low concentration vibrational probes.[56] The observed critical temperature T_c in the PhSeCN systems (BZP: 248 ± 2 K, OTP: 289 ± 2 K) was found to be depressed by about 2 K relative to literature values. This depression is consistent with the observed depression of T_g in the doped samples, as well as the depression of the analogous temperature T^* in doped isotropic phase nematic liquid crystal systems.[56] The fact that the slowest decay component of the FFCF obeys the ideal MCT scaling relationship for the α-relaxation time constant in both liquids strongly supports the assignment of t_{slow} as α-relaxation.

The reason why the α-relaxation is observed on a faster time scale in the 2D IR experiments than in other experiments is not clear. It is important to note that most other experiments, e. g., light scattering and OKE, measure an orientational correlation function that is intrinsically different from the FFCF, and therefore, the values obtained from different correlation functions would not be expected to be the same. However, the difference is greater than has been observed in other systems.[83,84] King *et al.* have suggested the difference in time scales between the FFCF and other observables is indicative of hierarchical dynamical slaving between the 2D IR t_{slow} and the α-relaxation observed with other experiments, ultimately due to the fractal-like, self-similar nature of the potential energy landscape.[82] In this view, the FFCF observable is reflecting the microscopic motions that are viewed collectively in other experiments that operate on a slower time scale. An alternative view, based on studies of the nematic-isotropic transition in liquid crystals,[55,56] suggests that 2D IR is sensitive to microscopic density fluctuations that are coupled to, but faster than, orientational fluctuations seen with other techniques. It is the nature of these density fluctuations that cause t_{slow} to decay on the faster-yet-proportional time scale to the α-relaxation measured with other methods.

In the Kubo model of the FFCF (Equation (4)), if $\Delta_i\tau_i < 1$, the component of the FFCF is motionally narrowed and a source of homogeneous broadening.[53] For a motionally narrowed contribution to the total FFCF, Δ_i and τ_i cannot be determined independently. Instead, the pure dephasing linewidth $\Gamma^* = \Delta^2\tau = 1/\pi T_2^*$ is obtained, where T_2^* is the pure dephasing time. The measured homogeneous dephasing time, T_2, also has contributions from population and orientational relaxation times, which are so slow that they are negligible in systems studied here.

The homogeneous linewidth Γ, which is caused by extremely fast, motionally narrowed dynamics, decreases substantially with decreasing temperatures. The values are given in the supplementary material, Tables SI–SIII. The trend is harder to see for the FlSeCN probe (Table SII) because of the limited range of temperatures studied. It is difficult to assign a definite reason for this drop because the homogeneous linewidth depends on both Δ, the range of frequencies sampled, and τ, the sampling time, and these two parameters cannot be measured independently. If a decrease in temperature caused only τ to slow, the homogeneous line would become wider, provided the structural fluctuations were still fast enough to cause motional narrowing. If τ slowed enough such that $\Delta\tau > 1$, then either a new fast component would appear in the spectral diffusion (CLS) or the amplitude of the fastest component would increase. Neither of these occurred. If as the temperature is lowered, Δ decreases substantially but τ only increases mildly, the homogeneous width will decrease because of increased motional narrowing. Such a decrease will not have an effect on the amplitudes or time constants of the spectral diffusion. This mechanism is reasonable but cannot be definitely proven.

The fastest relaxation time (t_{fast}), i.e., the faster time constant of the biexponential at higher temperatures and the fastest time constant of the triexponential at lower temperatures, occurs solely on the picosecond time scale and becomes a smaller component (Δ_1 becomes smaller) of the overall decay as the temperature is decreased, varying from >50% above T_m to ~15% at the lowest temperatures. The time constant, t_{fast}, has an Arrhenius temperature dependence within error, and can be fit with the appropriate functional form (Figure 6, dotted black lines)

$$\tau = \tau_0 \exp\left(\frac{E_a}{RT}\right), \tag{9}$$

to yield activation energies of 3.2 ± 0.6 kJ/mol and 3.9 ± 1.2 kJ/mol for OTP and BZP, respectively.

The nature of the t_{fast} process observed with the 2D IR experiments is less clear. The MCT fast β-process[6] is a possible candidate. This process is related to the intermolecular

motions of tightly caged molecules in potential energy minima.[1,12,85] 2D IR would be highly sensitive to such solvent shell dynamics.[57–59] The fast β-process usually appears on a few picosecond time scale with a weak temperature dependence as is observed for the 2D IR data, although it also generally appears as a power law in the MCT equations. This is again attributable to the differences in the FFCF from other correlators, and it has been previously demonstrated that a schematic MCT correlator is as capable of describing a multiexponential decay as a power law.[56] Thus, it is possible to attribute the t_{fast} exponential decay to processes MCT describes as power laws observed with other techniques.

However, the t_{fast} processes, in conjunction with motionally narrowed dynamics, are the dominant contributions to the absorption line shape at high temperatures. This seems potentially contrary to the generally subtle nature of the fast β-process. A possible alternative explanation is that t_{fast} is related to intramolecular processes of BZP and OTP, which are diffusive because of hindrance by the solvent as opposed to true vibrations that would occur in the gas phase. The relaxation rates of the internal degrees of freedom of OTP have been calculated and are on the order of several picoseconds at high temperature,[86] which is in good agreement with the 2D IR data and the literature.[87] These intramolecular motions are believed to obscure the nature of the true fast β-process predicted by MCT in OTP.[86,87]

Finally, the middle relaxation time (t_{mid}) comes into existence in the triexponential fit at lower temperatures, where it bifurcates from the t_{slow} process. The t_{slow} process continues to grow in a super-Arrhenius manner with decreasing temperature, while the t_{mid} process is the Arrhenius continuation of the t_{slow} process from higher temperatures. t_{mid} is then a potential example of the onset of a secondary relaxation in glass forming liquids. Fitting t_{mid} as a continuation of t_{slow} with Equation (9) (Figure 6, solid red lines) yields activation energies of 25.8 ± 1.8 kJ/mol for OTP and 16.3 ± 2.3 kJ/mol for BZP.

As examined in Sec. III C 1, the temperature where t_{mid} appears in the triexponential model marks a dynamic crossover that is independent of the choice of model. Although statistical analysis supports the triexponential model for the deeply supercooled 2D IR data, a transition occurs at this temperature either way, as the α-relaxation must either bifurcate into two separate relaxations (triexponential model) or become a broad distribution of relaxation times (exponential plus stretched exponential model). In both liquids, this crossover occurs at a temperature that is well above the T_c that is calculated from t_{slow}. The crossover occurs at ~1.3 T_g, which is 275 K for BZP doped with PhSeCN, or 315 K for OTP doped with PhSeCN. This temperature also corresponds to approximately the temperature where t_{slow} ceases to have an Arrhenius temperature dependence, as shown by the solid red lines in Figure 6. All of this is consistent with the crossover temperature being the onset temperature T_o, as predicted from computational models of the potential energy landscape of glass forming liquids,[21,22] i.e., the temperature where some (but not all) particles in the liquid are unable to relax independently, requiring activated relaxation pathways.

Beyond the lifetime density analysis results presented above, the observed thermodynamics of this intermediate process may provide additional support for its physical nature. t_{mid} appears as the Arrhenius continuation of the higher temperature t_{slow} process. This behavior is consistent with the potential energy landscape picture already described. Below T_o but above T_c, while some of the liquid is influenced by the landscape and unable to relax independently, some of the liquid is still able to independently relax. With the presence of these two subensembles, one of them should be a subpopulation that relaxes with the same Arrhenius temperature dependence as at higher temperatures. In real space, the presence of these two subensembles would be manifested as non-ergodic diffusive motion of mobile particles that are loosely caged by their less-mobile neighbors.[85,88] Ultimately, it is the motion of these mobile particles that provide pathways that allow the less-mobile neighbors to eventually relax, i.e., activated relaxation.

The fact that t_{mid} is a separate decay may indicate that it is a slow β (Johari-Goldstein) relaxation.[41] Slow β-relaxations bifurcate from the α-relaxation with decreasing temperature, are tightly associated with dynamic heterogeneity and activated dynamics, and have activation energies consistent with interbasin potential energy landscape transitions.[85,89] All of these features are consistent with the t_{mid} process observed here. Further, slow β-relaxation has been observed in atomic glasses through mechanical relaxation mechanisms.[88] As atoms lack orientational degrees of freedom, the slow β-relaxation mechanism must be at least in part translational. The decoupling of translational and rotational diffusion is known to appear at mild supercooling (above T_c) in simulations[12,90–92] and has been previously connected with T_o,[93,94] which is the temperature regime where t_{mid} is first resolved. Spectral diffusion has been observed previously to occur through fast density fluctuations, especially when orientational relaxation becomes very slow, such as in the isotropic phase of liquid crystals near the isotropic to nematic phase transition.[55,56] Density fluctuations provide a possible mechanistic origin of the relaxation as seen in the 2D IR data.

This interpretation of t_{mid} places the onset temperature of the slow β-relaxation at T_o and necessitates that the β-relaxation changes to a stronger temperature dependence closer to T_g in order to match data from other spectroscopies. The onset of the slow β-relaxation has been commonly attributed to T_c from extrapolation of relaxation times from below T_g to warmer temperatures.[3,4,13–16] However, there is more recent evidence that the slow β-relaxation does change its temperature dependence to super-Arrhenius slightly above T_g, including in BZP.[39,95] This evidence has led to alternative models that predict a merger with the α-relaxation at higher temperatures, including at T_o.[24,95,96] This picture is again consistent with density fluctuations, at least in part, being the origin of the slow β-relaxation and translational-rotational decoupling at T_o.

IV. CONCLUDING REMARKS

2D IR vibrational spectroscopy with long-lived vibrational probes was shown capable of measuring a wide range

of supercooled liquid dynamics, ranging from slow, super-Arrhenius behavior to ultrafast dynamics. The results confirm previous studies of spectral diffusion that show an α-like relaxation can be observed, which obeys the ideal MCT scaling law while acting on a faster time scale. A mildly temperature dependent picosecond time scale relaxation was also found, which is reminiscent of the fast β-process predicted by MCT, or other molecular scale processes that have been implicated in masking such dynamics. Significantly, a well-defined crossover temperature was observed, which marks the point where the biexponential FFCF at high temperatures was no longer sufficient to describe the dynamics. This crossover occurred well above the MCT critical temperature, as determined from the ideal MCT scaling law, and instead coincides with the onset temperature T_o, corresponding to the point where the α-relaxation becomes super-Arrhenius and the onset of dynamic heterogeneity.

Using lifetime density analysis, a numerical inverse Laplace transform, it was determined that the crossover is best described as the splitting off of a separate decay process from the α-relaxation. This splitting, along with its association with density fluctuations that 2D IR is known to be sensitive to, led to the association of this intermediate relaxation process with the slow β-relaxation of Johari and Goldstein. The connections between the slow β-relaxation, density fluctuations, and the onset of rotational-translational decoupling, dynamical heterogeneity, and potential energy landscape changes at the temperature T_o relate the temperature dependence of the observed spectral diffusion to a consistent mechanistic picture of the nature of liquids at deep supercooling temperatures.

SUPPLEMENTARY MATERIAL

See the supplementary material for (A) polarization dependence, (B) tables of fit parameters, and (C) vibrational probe synthesis.

ACKNOWLEDGMENTS

This work was supported by the Division of Chemistry, Directorate of Mathematical and Physical Sciences, National Science Foundation (NSF) (No. CHE-1461477). We thank A. Tamimi for helpful discussions.

[1] C. A. Angell, Science **267**, 1924–1935 (1995).
[2] P. G. Debenedetti and F. H. Stillinger, Nature **410**, 259–267 (2001).
[3] C. A. Angell, K. L. Ngai, G. B. McKenna, P. F. McMillan, and S. W. Martin, J. Appl. Phys. **88**, 3113–3157 (2000).
[4] R. Richert, J. Phys.: Condens. Matter **14**, R703–R738 (2002).
[5] D. Chandler and J. P. Garrahan, Annu. Rev. Phys. Chem. **61**, 191–217 (2010).
[6] W. Götze and L. Sjögren, Rep. Prog. Phys. **55**, 241–376 (1992).
[7] W. Götze and L. Sjögren, Transp. Theory Stat. Phys. **24**, 801–853 (1995).
[8] M. D. Ediger, C. A. Angell, and S. R. Nagel, J. Phys. Chem. **100**, 13200–13212 (1996).
[9] K. L. Ngai, J. Non-Cryst. Solids **275**, 7–51 (2000).
[10] P. Lunkenheimer, U. Schneider, R. Brand, and A. Loidl, Contemp. Phys. **41**, 15–36 (2000).
[11] V. Lubchenko and P. G. Wolynes, Annu. Rev. Phys. Chem. **58**, 235–266 (2007).
[12] L. Berthier and J. P. Garrahan, Phys. Rev. E **68**, 041201 (2003).
[13] C. A. Angell, J. Phys.: Condens. Matter **12**, 6463–6475 (2000).
[14] C. Hansen, F. Stickel, T. Berger, R. Richert, and E. W. Fischer, J. Chem. Phys. **107**, 1086 (1997).
[15] E. Rössler, Phys. Rev. Lett. **65**, 1595–1598 (1990).
[16] E. Rössler, U. Warschewske, P. Eiermann, A. P. Sokolov, and D. Quitmann, J. Non-Cryst. Solids **172-174**, 113–125 (1994).
[17] I. Chang and H. Sillescu, J. Phys. Chem. B **101**, 8794–8801 (1997).
[18] M. T. Cicerone and M. D. Ediger, J. Chem. Phys. **104**, 7210–7218 (1996).
[19] F. Fujara, B. Geil, H. Sillescu, and G. Fleischer, Z. Phys. B: Condens. Matter **88**, 195–204 (1992).
[20] M. T. Cicerone, F. R. Blackburn, and M. D. Ediger, J. Chem. Phys. **102**, 471 (1995).
[21] S. Sastry, P. G. Debenedetti, and F. H. Stillinger, Nature **393**, 554–557 (1998).
[22] Y. Brumer and D. R. Reichman, Phys. Rev. E **69**, 041202 (2004).
[23] F. Mallamace, C. Branca, C. Corsaro, N. Leone, J. Spooren, S.-H. Chen, and H. E. Stanley, Proc. Natl. Acad. Sci. U. S. A. **107**, 22457–22462 (2010).
[24] H. Tanaka, Phys. Rev. E **69**, 021502 (2004).
[25] A. Jaiswal, S. O'Keeffe, R. Mills, A. Podlesnyak, G. Ehlers, W. Dmowski, K. Lokshin, J. Stevick, T. Egami, and Y. Zhang, J. Phys. Chem. B **120**, 1142–1148 (2016).
[26] G. Hinze, D. D. Brace, S. D. Gottke, and M. D. Fayer, Phys. Rev. Lett. **84**, 4783 (2000).
[27] S. D. Gottke, D. D. Brace, G. Hinze, and M. D. Fayer, J. Phys. Chem. B **105**, 238–245 (2001).
[28] H. Cang, V. N. Novikov, and M. D. Fayer, J. Chem. Phys. **118**, 2800–2807 (2003).
[29] H. Cang, V. N. Novikov, and M. D. Fayer, Phys. Rev. Lett. **90**, 197401 (2003).
[30] A. Brodin and E. A. Rössler, J. Chem. Phys. **125**, 114502 (2006).
[31] H. Z. Cummins, Y. H. Hwang, G. Li, W. M. Du, W. Losert, and G. Q. Shen, J. Non-Cryst. Solids **235-237**, 254–267 (1998).
[32] H. Z. Cummins, G. Li, W. Du, Y. H. Hwang, and G. Q. Shen, Prog. Theor. Phys. Suppl. **126**, 21–34 (1997).
[33] W. Steffen, G. Meier, and A. Patkowski, Phys. A **201**, 300–304 (1993).
[34] W. Steffen, A. Patkowski, H. Gläser, G. Meier, and E. W. Fischer, Phys. Rev. E **49**, 2992–3002 (1994).
[35] F. Mallamace, C. Corsaro, N. Leone, V. Villari, N. Micali, and S.-H. Chen, Sci. Rep. **4**, 3747 (2014).
[36] N. Petzold and E. A. Rössler, J. Chem. Phys. **133**, 124512 (2010).
[37] N. A. Davydova, V. I. Mel'nik, J. Baran, and M. Drozd, J. Mol. Struct. **651-653**, 171–175 (2003).
[38] T. Hikima, Y. Adachi, M. Hanaya, and M. Oguni, Phys. Rev. B **52**, 3900–3908 (1995).
[39] P. Lunkenheimer, L. C. Pardo, M. Köhler, and A. Loidl, Phys. Rev. E **77**, 031506 (2008).
[40] L. C. Pardo, P. Lunkenheimer, and A. Loidl, Phys Rev E **76**, 030502 (2007).
[41] G. P. Johari and M. Goldstein, J. Chem. Phys. **53**, 2372–2388 (1970).
[42] R. Richert, J. Chem. Phys. **123**, 154502 (2005).
[43] H. Wagner and R. Richert, J. Phys. Chem. B **103**, 4071–4077 (1999).
[44] E. Rössler, K. Börner, J. Tauchert, M. Taupitz, and M. Pöschl, Ber. Bunsengesellschaft phys. Chem. **95**, 1077–1084 (1991).
[45] A. Tölle, Rep. Prog. Phys. **64**, 1473–1532 (2001).
[46] A. Tölle, H. Schober, J. Wuttke, and F. Fujara, Phys. Rev. E **56**, 809–815 (1997).
[47] W. Petry, E. Bartsch, F. Fujara, M. Kiebel, H. Sillescu, and B. Farago, Z. Phys. B: Condens. Matter **83**, 175–184 (1991).
[48] P. D. Hyde, T. E. Evert, M. T. Cicerone, and M. D. Ediger, J. Non-Cryst. Solids **131-133**, 42–47 (1991).
[49] M. Saito, S. Kitao, Y. Kobayashi, M. Kurokuzu, Y. Yoda, and M. Seto, Phys. Rev. Lett. **109**, 115705 (2012).
[50] V. Bercu, M. Martinelli, C. A. Massa, L. A. Pardi, E. A. Rössler, and D. Leporini, J. Chem. Phys. **129**, 081102 (2008).
[51] P. D. Hyde, T. E. Evert, and M. D. Ediger, J. Chem. Phys. **93**, 2274–2279 (1990).
[52] S. Mukamel, *Principles of Nonlinear Optical Spectroscopy* (Oxford University Press, New York, 1995).
[53] S. Mukamel, Annu. Rev. Phys. Chem. **51**, 691–729 (2000).
[54] S. Park, K. Kwak, and M. D. Fayer, Laser Phys. Lett. **4**, 704–718 (2007).
[55] K. P. Sokolowsky, H. E. Bailey, and M. D. Fayer, J. Chem. Phys. **141**, 194502 (2014).
[56] K. P. Sokolowsky, H. E. Bailey, D. J. Hoffman, H. C. Andersen, and M. D. Fayer, J. Phys. Chem. B **120**, 7003–7015 (2016).
[57] A. Tamimi, H. E. Bailey, and M. D. Fayer, J. Phys. Chem. B **120**(30), 7488–7501 (2016).
[58] A. Tamimi and M. D. Fayer, J. Phys. Chem. B **120**(26), 5842–5854 (2016).

[59]R. Yuan, C. Yan, A. Tamimi, and M. D. Fayer, J. Phys. Chem. B **119**(42), 13407–13415 (2015).
[60]M. Maj, K. Kwak, and M. Cho, ChemPhysChem **16**, 3468–3476 (2015).
[61]K. P. Sokolowsky and M. D. Fayer, J. Phys. Chem. B **117**, 15060–15071 (2013).
[62]C. Slavov, H. Hartmann, and J. Wachtveitl, Anal. Chem. **87**, 2328–2336 (2015).
[63]R. D. McCulla and W. S. Jenks, J. Am. Chem. Soc. **126**, 16058–16065 (2004).
[64]J. Zheng, K. Kwak, and M. D. Fayer, Acc. Chem. Res. **40**, 75–83 (2007).
[65]P. L. Kramer, J. Nishida, and M. D. Fayer, J. Chem. Phys. **143**, 124505 (2015).
[66]P. L. Kramer, J. Nishida, C. H. Giammanco, A. Tamimi, and M. D. Fayer, J. Chem. Phys. **142**, 184505 (2015).
[67]P. L. Kramer, C. H. Giammanco, A. Tamimi, D. J. Hoffman, K. P. Sokolowsky, and M. D. Fayer, J. Opt. Soc. Am. B **33**, 1143 (2016).
[68]K. Kwak, D. E. Rosenfeld, and M. D. Fayer, J. Chem. Phys. **128**(20), 204505 (2008).
[69]R. Kubo, in *Fluctuation, Relaxation, and Resonance in Magnetic Systems*, edited by D. Ter Haar (Oliver and Boyd, London, 1961).
[70]K. Kwak, S. Park, I. J. Finkelstein, and M. D. Fayer, J. Chem. Phys. **127**(12), 124503 (2007).
[71]F. Perakis and P. Hamm, J. Phys. Chem. B **115**, 5289–5293 (2011).
[72]D. Czurlok, M. von Domaros, M. Thomas, J. Gleim, J. Lindner, B. Kirchner, and P. Vöhringer, Phys. Chem. Chem. Phys. **17**, 29776–29785 (2015).
[73]H. Maekawa, S. Sul, and N.-H. Ge, Chem. Phys. **422**, 22–30 (2013).
[74]A. Lapini, M. Pagliai, S. Fanetti, M. Citroni, S. Scandolo, R. Bini, and R. Righini, J. Phys. Chem. Lett. **7**, 3579–3584 (2016).
[75]K. Adamczyk, M. Candelaresi, K. Robb, A. Gumiero, M. a. Walsh, A. W. Parker, P. A. Hoskisson, N. P. Tucker, and N. T. Hunt, Meas. Sci. Technol. **23**, 062001 (2012).
[76]M. A. Navakatikyan, J. Exp. Anal. Behav. **87**, 121–141 (2007).
[77]U. Bengtzelius, W. Götze, and A. Sjolander, J. Phys. C: Solid State Phys. **17**, 5915–5934 (2000).
[78]H. Cang, J. Li, H. C. Andersen, and M. D. Fayer, J. Chem. Phys. **123**, 064508 (2005).
[79]W. Götze and M. Sperl, Phys. Rev. Lett. **92**, 105701 (2004).
[80]H. Cang, J. Li, V. N. Novikov, and M. D. Fayer, J. Chem. Phys. **118**, 9303–9311 (2003).
[81]J. Li, I. Wang, K. Fruchey, and M. D. Fayer, J. Phys. Chem. A **110**, 10384–10391 (2006).
[82]J. T. King, M. R. Ross, and K. J. Kubarych, Phys. Rev. Lett. **108**, 157401 (2012).
[83]D. Laage, Science **311**, 832–835 (2006).
[84]D. Laage and J. T. Hynes, J. Phys. Chem. B **112**, 14230–14242 (2008).
[85]M. T. Cicerone, Q. Zhong, and M. Tyagi, Phys. Rev. Lett. **113**, 117801 (2014).
[86]S. Mossa, G. Monaco, and G. Ruocco, Europhys. Lett. **60**, 92–98 (2002).
[87]G. Monaco, S. Caponi, R. Di Leonardo, D. Fioretto, and G. Ruocco, Phys. Rev. E **62**, 7595 (2000).
[88]G. P. Johari, J. Non-Cryst. Solids **307-310**, 317–325 (2002).
[89]M. Goldstein, J. Chem. Phys. **132**, 041104 (2010).
[90]W. Kob and H. C. Andersen, Phys. Rev. Lett. **73**, 1376–1379 (1994).
[91]W. Kob and H. C. Andersen, Phys. Rev. E **52**, 4134–4153 (1995).
[92]W. Kob and H. C. Andersen, Phys. Rev. E **51**, 4626–4641 (1995).
[93]A. Jaiswal, T. Egami, and Y. Zhang, Phys. Rev. B **91**, 134204 (2015).
[94]A. Jaiswal, S. O'Keeffe, R. Mills, A. Podlesynak, G. Ehlers, W. Dmowski, K. Lokshin, J. Stevick, T. Egami, and Y. Zhang, J. Phys. Chem. B **120**, 1142–1148 (2016).
[95]K. L. Ngai and M. Paluch, J. Chem. Phys. **120**, 857–873 (2004).
[96]K. L. Ngai, J. Phys.: Condens. Matter **15**, S1107–S1125 (2003).